Peer-reviewed version available at Arabian Journal for Science and Engineering 2018; doi:10.1007/s13369-018-3210-6

Article

Three-Dimensional Modeling Interaction of Shock Wave with Fin at Mach 5

Amjad A. Pasha

Department of Aeronautical Engineering, King Abdul Aziz University, Jeddah-21589, Saudi Arabia; aapasha@kau.edu.sa

Abstract: The three-dimensional single fin configuration finds application in an intake geometry where the cowl-shock wave interacts with the side-wall boundary-layer. Accurate numerical simulation of such three-dimensional shock/turbulent boundary-layer interaction flows, which are characterized by the appearance of strong crossflow separation, is a challenging task. Reynolds-averaged Navier-Stokes computations using the shock-unsteadiness modified Spalart-Allmaras model is carried out at Mach of 5 at large fin angle of 23°. The computed results using the modified model are compared to the standard Spalart-Allmaras model and validated against the experimental data. The focus of work is to implement the modified model and to study the flow physics in detail in the complex region of swept-shock-wave turbulent boundary-layer interaction in terms of the shock structure, expansion fan, shear layer and the surface streamlines. The flow structure is correlated to the wall pressure and skin friction in detail. It is observed that the standard model predicts an initial pressure location downstream of the experiments. The modified model reduces the eddy viscosity at the shock and predicts close to the experiments. Overall, the surface pressure using modified model is predicted accurately at all the locations. The skin friction is under predicted by both the models in the reattachment region and is attributed to the poor performance of turbulence models due to flow laminarization.

Keywords: high speed flows; shock wave; turbulent boundary layer; shock-unsteadiness; separation bubble; turbulence modeling; single fin

---

Nomenclature

b_1'	=	shock-unsteadiness damping parameter
C_f	=	skin friction coefficient
c_{b_1}'	=	shock-unsteadiness parameter
M_{1n}	=	upstream Mach number normal to shock
y_2^+	=	wall-normal distance to the nearest point in wall coordinates
δ_0	=	boundary-layer thickness upstream of interaction
μ_T	=	eddy viscosity
ν	=	kinematic molecular viscosity
$\tilde{\nu}$	=	modified turbulent kinematic viscosity
subscripts		
0	=	stagnation condition
n	=	normal to shock wave
w	=	wall condition
∞	=	freestream condition
abbreviation		
CFL	=	CourantFriedrichsLewy
SA	=	Spalart-Allmaras

1. Introduction

The most fundamental three-dimensional shock/boundary-layer interaction is generated on a single fin configuration. It consists of a flat plate with a sharp fin mounted perpendicular to it. The oblique shock wave generated by the fin interacts with the turbulent boundary layer on the plate and results in flow separation. The three-dimensional vortical flow thus generated alters the inviscid flow pattern. Additional shock waves, expansion regions and free shear layers are generated that result in a complex flow in the interaction region. Practical applications of single fin configuration include scramjet inlets, where the oblique shock generated by the cowl interacts with the side wall boundary layer.

The single fin shock boundary-layer interaction flows are characterized by localized regions of increased pressure, skin friction and heat transfer rate. Prediction of these surface properties is important in the design of scramjet inlets. In addition, the flow distortion caused by the interaction can degrade the performance of these inlets significantly. Therefore the aerodynamic loads generated from these interactions play a significant role in the structural integrity of hypersonic vehicle [1,2]. Computational fluid dynamic approach is a useful tool to understand the complex three-dimensional flow pattern in these shock-wave/boundary-layer interactions and to predict its influence on the wall data. The direct numerical simulation and large eddy simulation demand a large number of grid points at high Reynolds number flows leading to large computational resources and computational times to capture the fine features of shock-wave/turbulent boundary-layer interaction cases [3]. As an engineering approach, Reynolds-averaged Navier-Stokes (RANS) method is applied in the present work along with one-equation turbulence models to compute these flowfields.

Experiments and computations were carried by many authors [4–9] for single fin geometry. Panaras [9] computed using RANS code for deflection angle of $\beta = 20^\circ$ and $M_\infty = 3.0$. The wall pressure data was improved using modified Baldwin-Lomax model compared as to the standard Baldwin-Lomax model. Edwards et al. [6] studied the performance of four different one-equation turbulence models for $M_\infty = 8$ and $\theta = 15^\circ$. Among them the standard Spalart-Allmaras model has shown to predict the surface properties close to the experiments. Thivet [8] computed three different single fin configuration cases with $M_\infty = 3$, $\theta = 15^\circ$, $M_\infty = 4$, $\theta = 20^\circ$ and $M_\infty = 4$, $\theta = 30.6^\circ$, using the standard and modified k-ω models. The prediction of secondary vortex region was improved using modified k-ω model, hence improving the wall data in this region. The review articles [10–15] discusses different single fin configurations flow physics and wall data in detail.

The shock-unsteadiness modified Spalart-Allmaras model of Sinha et al. [16] has shown potential in improving separation bubble prediction in two-dimensional supersonic compression corner flows and axisymmetric hypersonic cone-flare flows [17]. In this paper, an attempt is made to extend this model to three-dimensional single fin configuration flows and study the flowfield in detail. First, the test case is described, which is followed by the simulation methodology. Next, the flowfield is explained for the strongest shock strength case with fin deflection angle of 23° and $M_\infty = 5$ using modified Spalart-Allmaras model. Next, the computed wall pressure and skin friction using modified model [16] and the standard model [18] is compared with the experimental results [19].

2. Test case

The schematic of the single fin configuration used in the experiments of Schulein [19] is shown in Figure 1. The fin is inclined with a deflection angle of $\theta = 23^\circ$ to the flow direction at $M_\infty = 5$. The stagnation temperature of $T_0 = 410$ K and stagnation pressure $P_0 = 2.12$ MPa were taken in the reservoir of the Ludweig tube experimental facility. A fin of height = 100 mm normal to the flat plate is taken. The fin tip is placed at a distance of 286 mm downstream of the flat plate edge. Both the flat plate and fin wall are maintained under the isothermal condition of 300 K. The flow is turbulent, upstream of the interaction region with a unit Reynolds number of $Re_{1\infty} = 37 \times 10^6$ m^{-1}. Wall data like pressure, skin friction and heat transfer rates were measured at different cross sections in the shock-wave/turbulent boundary-layer interaction region (see Figure 1). The undisturbed turbulent

boundary-layer properties were measured on the flat plate at a distance of 20 mm upstream of the fin tip. The boundary layer thickness δ of 3.8 mm, displacement thickness = 1.6 mm, momentum thickness = 0.16 mm and skin friction $C_f = 1.35 \times 10^{-3}$ is measured.

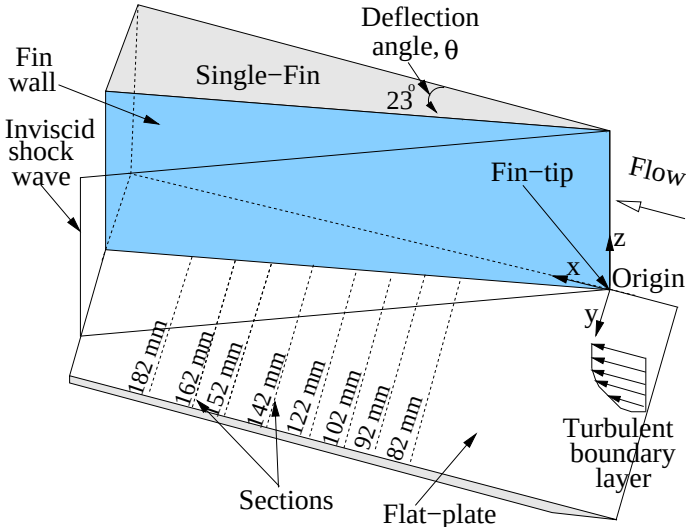

Figure 1. Three-dimensional single fin configuration with fin mounted on the flat plate. The surface measurements [19] were taken along the dashed lines.

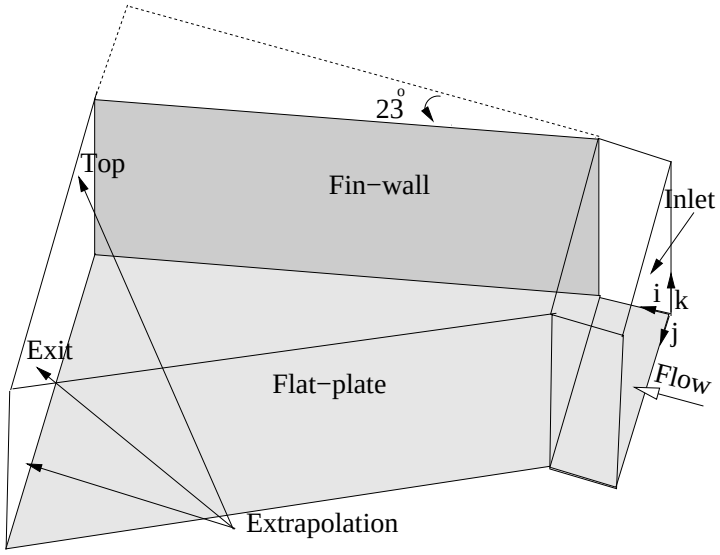

Figure 2. Computational domain with appropriate boundary conditions.

3. Simulation methodology

The three-dimensional Reynolds-averaged Navier-Stokes equations [20] are taken in the numerical simulations. The turbulence model equations are fully coupled to the mean flow equations. The shock-unsteadiness modified Spalart-Allmaras model of Sinha et al. [16] and its standard version [18] is used for calculating the eddy viscosity. A compressible correction to standard Spalart-Allmaras model has been proposed by Catris et al. [25] by modifying the diffusion laws in the turbulence model, but this strategy complicates the numerical implementation for three-dimensional flows [26]. The governing equations are discretized in a finite-volume formulation

where the inviscid fluxes are computed using a modified low-dissipation form of the Steger-Warming flux-splitting approach. The method is second-order accurate both in stream wise and wall-normal directions. The viscous fluxes and the turbulent source terms are evaluated using central difference method. More details of the numerical method are given in Ref. [21]. The code is capable of running on parallel machines and has been used successfully in several supersonic and hypersonic applications [16,17,22,23].

The shock-unsteadiness modified Spalart-Allmaras model of Sinha et al. [16] accounts for the effect of unsteady shock motion in a steady mean flow. The shock-unsteadiness correction is achieved by adding a source term of the form $-c'_{b_1}\bar{\rho}\tilde{\nu}S_{ii}$ in the transport equation for $\bar{\rho}\tilde{\nu}$, where $\bar{\rho}$ is mean density $\tilde{\nu}$ is modified turbulent kinematic viscosity, S_{ii} is mean dilatation and shock-unsteadiness parameter

$$c'_{b_1} = \frac{4}{3}(1 - b'_1) - \frac{2}{3}c'_{\epsilon 1}. \tag{1}$$

Note that this additional term is effective only in regions of strong dilatation and therefore does not alter the standard Spalart-Allmaras model [18] elsewhere. Here, b'_1 is model parameter and $c'_{\epsilon 1} = 1.25 + 0.2(M_{1n} - 1)$. The model parameter b'_1 represents the coupling between the unsteady shock motion and the upstream velocity fluctuations, and is given by,

$$b'_1 = \max\left[0,\ 0.4\left(1 - e^{1-M_{1n}}\right)\right] \tag{2}$$

It is zero for subsonic flows without shock waves and it reaches an asymptotic value of 0.4 for high Mach numbers. The detailed formulation of shock-unsteadiness modified Spalart-Allmaras model and its implementation for two-dimensional compression corner and axisymmetric cone-flare flows at supersonic and hypersonic Mach numbers is presented in Refs. [16,17]. In the current work, the modification is applied to the three-dimensional flows which are more difficult to simulate as compared to their counterpart two-dimensional flows.

The computational domain and boundary conditions for three-dimensional single fin configuration are identified in Figure 2. The freestream conditions taken in the simulations are $T_\infty = 68.3$ K and $p_\infty = 4008.5$ Pa. At the fin wall and flat plate, a constant wall temperature of 300 K and no-slip velocity condition is applied. An extrapolation boundary condition is assigned at top and exit planes. The freestream and wall boundary conditions for the turbulence model variables are taken as $\tilde{\nu}_\infty = 0.1\ \nu_\infty$ and $(\nu_T)_w = 0$. Inlet profiles for the computations are obtained from separate two-dimensional flat plate simulation at the freestream and wall boundary conditions identical to those listed above. The value of the momentum thickness reported in the experiments [19] is matched to obtain the mean flow and the turbulence profiles at the inlet boundary of the computational domain.

A single-block grid is generated using a code and a careful grid refinement study is performed by systematically varying the number of grid points in each direction, as well as refining the cell size in critical regions. The origin is taken at a tip of the single fin and the grid is stretched exponentially in the upstream and downstream directions of origin with initial grid size of 1×10^{-4} m. A structured mesh with exponential stretching normal to the plate and fin walls are used to span the computational domain. Wall pressure and skin friction coefficient are found to be sensitive to the computational mesh and are used to identify a grid converged solution. First, the number of points in the wall parallel direction is refined and it is observed that among the three grids, the $100 \times 110 \times 110$, $140 \times 110 \times 110$, and $200 \times 110 \times 110$, the last two grids match. Next, $140 \times 110 \times 110$ grid is taken and only the distance of the first cell center from the wall is successively reduced by halve-times from its initial value of 2×10^{-6} m. Wall pressure and C_f variation indicate that 1×10^{-6} m is sufficient for an accurate solution. The y_2^+ varies between 0.06 in the undisturbed boundary-layer o a maximum value of $y_2^+ < 0.6$ in the shock/boundary-layer interaction region. This value of the y_2^+ is sufficient to capture the high gradients of the mean and turbulent variables in the boundary layer in the

wall-normal direction, especially at the reattachment region. In the next step, using $140 \times 110 \times 110$ grid, the number of points in the transverse direction is increased. It is observed that variation in wall pressure and skin friction for $140 \times 160 \times 110$ and $140 \times 200 \times 110$ is less than 3%. Finally, the number of points in the flat plate normal direction is increased to arrive at the $140 \times 160 \times 160$ grid. Surface properties variation shows that further refinement to $140 \times 160 \times 200$ grid points yields less than 2% variation in wall pressure and skin friction. A converged grid of $140 \times 160 \times 160$ is obtained with 140 points along the streamwise direction, 160 points transverse to the flow and 160 points normal to the plate.

In the present computations, a CFL of 0.05 is used at the beginning and it is gradually increased to 10 in the first 3500 iterations. It is further increased to 100 at 6000 iterations and to 1000 at 8000 iterations. A maximum CFL of 5000 is used after 10000 iterations. The corresponding time steps vary from 2×10^{-12} sec for the initial iterations to 2×10^{-5} sec at steady state solution. It takes 190 cpu-hours to reach the steady state solution in 30,000 iterations.

4. Flow physics

In this section, the computed results using modified Spalart-Allmaras model are discussed. An isometric view of the flow solution for the fin is shown in Figure 3. The pressure contours are taken at two x-sections of 92 and 182 mm to identify the shock structure. The flow pattern is indicated by the streamlines taken in the cell adjacent to the flat plate and behave similarly to the skin friction lines. A planar shock-wave generated by the fin interacts with the turbulent boundary-layer on the plate. It separates the boundary-layer and results in the formation of the separation shock. The flow separates at the primary separation line S1 and attaches at the primary reattachment line R1 near the fin wall. The streamlines converge at separation line S1 and the fluid moves upwards normal to the plate and then turns in a counter clockwise direction to form a helical flow as shown in Figure 4. Two stream surfaces originating at $z/\delta_0 = 0.8$ and $z/\delta_0 = 0.25$ are shown, where z is the normal distance from the plate and δ_0 is the undisturbed boundary-layer thickness. The fluid impinges on the plate at the reattachment line from the top, making the streamlines diverge in either direction. The inviscid shock-wave in Figure 4 bifurcates into a lambda structure and encloses the vortex region.

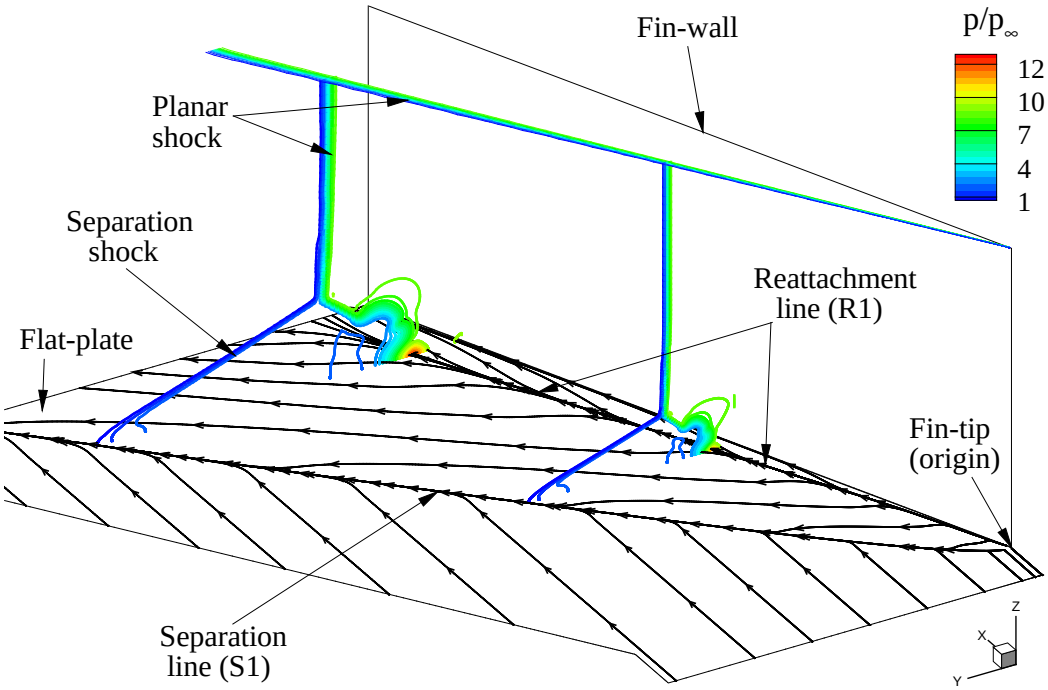

Figure 3. Flow solution in a single fin shock/boundary-layer interaction in terms of the computed surface streamlines on the plate. The shock structure is shown by pressure contours at x-sections = 92 mm and 182 mm.

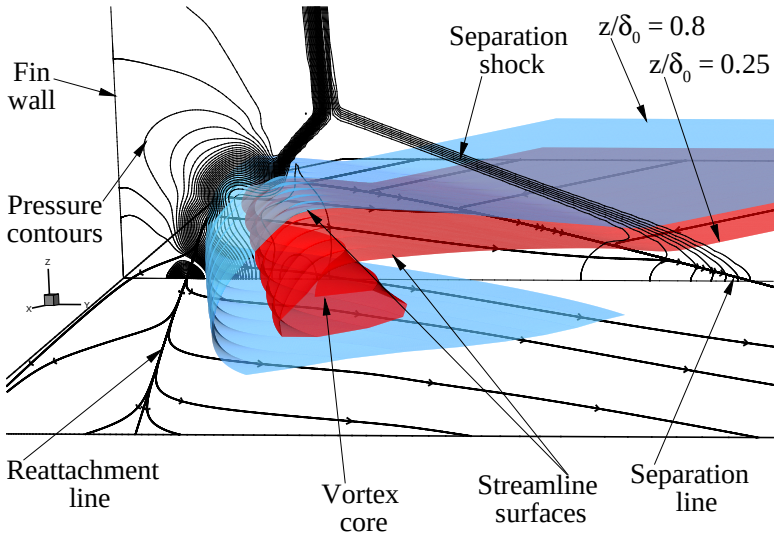

Figure 4. Computed stream-surfaces starting at $z/\delta_0 = 0.8$ and $z/\delta_0 = 0.25$ showing vortex region, and the pressure contours at x-section = 82 mm, as viewed from the downstream direction.

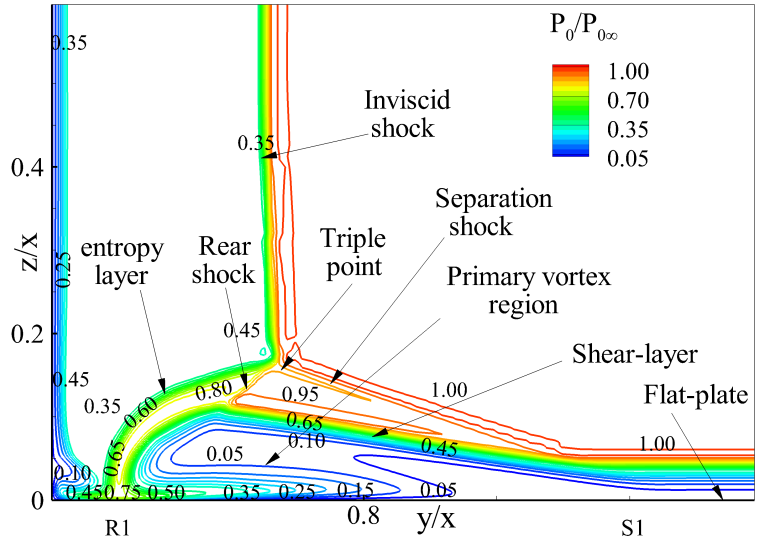

Figure 5. Computed stagnation pressure contours at x-section = 122 mm.

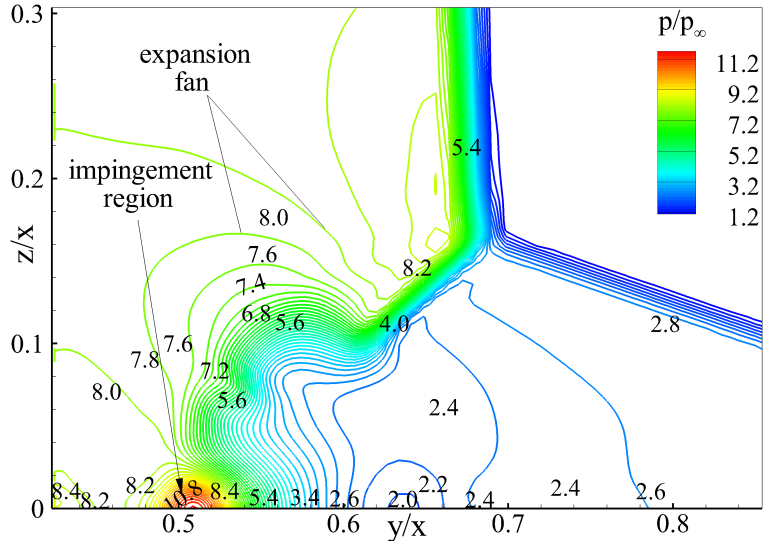

Figure 6. Enlarged region of computed pressure contours at x-section = 122 mm.

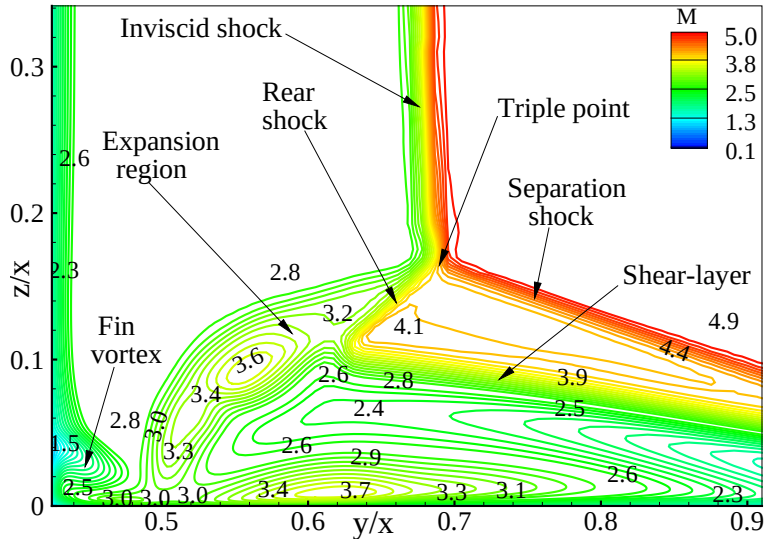

Figure 7. Enlarged region of computed Mach contours at x-section = 122 mm.

The computed stagnation pressure contours in Figure 5 indicate that an inviscid shock bifurcates and forms a separation shock and a rear shock, and results in the formation of lambda structure in a cross plane perpendicular to the freestream flow direction. The shear-layer is formed over the vortex region, which emanates from the separation point. It interacts with the rear shock-wave and then rolls up and turns back to form a tongue. An entropy layer is generated from the triple point of the intersection of three shock waves and a set of compression and expansion waves are formed between the shear layer and the slip line (see Figure 7). A secondary flow separation region was observed in the experiments [19], whereas in the present computation, it is not predicted. The computed pressure contours in Figure 6 indicate that an expansion fan is generated when the rear shock-wave reflects from the shear layer. The computed Mach contours in Figure 7 shows that a type-IV shock-shock interaction [24] is observed at the triple point. An alternate increase and decrease in Mach contours in the region between shear layer and jet represents the weak compression and expansion waves. The flow remains supersonic in the separated region. Small subsonic pockets are observed near the corner region of fin wall and plate. The impingement of the supersonic jet (entropy layer) emanating from the triple pointof shock-shock interaction results in peak values of pressure as indicated in the region marked in Figure 6. A small fin-vortex is formed when the fluid coming from the inviscid region interacts with fin wall and turns in the clockwise direction, as viewed from the downstream direction. Similar, corner-vortex was observed in the vapor screen images of the experiments [4]. The schematic sketches of these flowfield features are explained in detail in Refs. [5,14].

5. Comparison of computed wall data with experiments

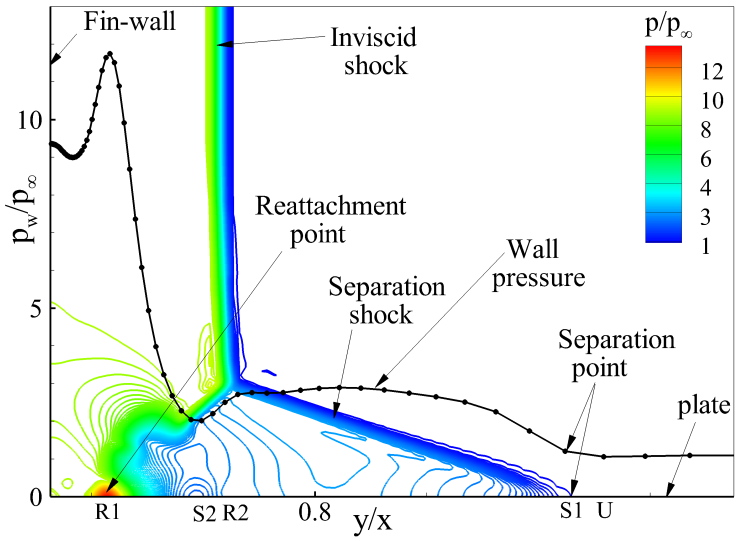

Figure 8. Computed pressure contours overlapped with wall pressure at x-section = 122 mm.

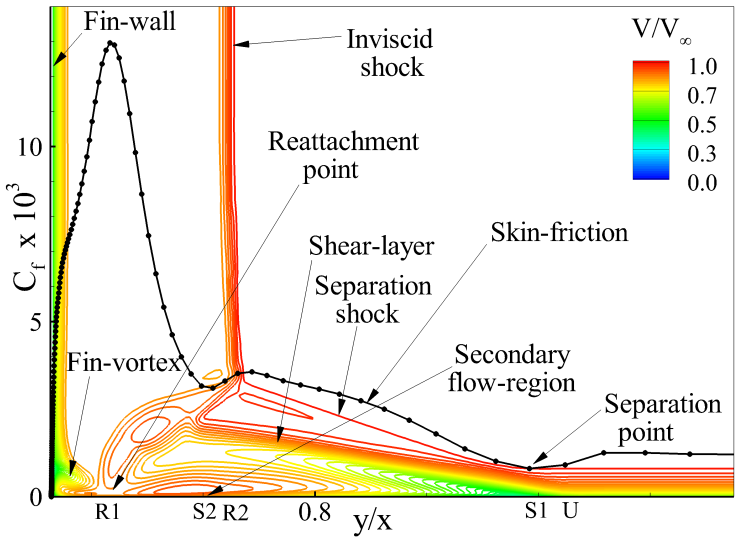

Figure 9. Computed speed contours overlapped with skin friction coefficient at x-section = 122 mm.

Figures 8 and 9 shows the computed pressure and speed contours, overlapped with the wall pressure and skin friction on the flat plate at x-section = 122 mm. The distance along the y-axis is normalized with the corresponding x-section distance measured from the fin tip. The surface data is taken along the dashed lines as shown in Figure 1. The wall pressure remains constant in the undisturbed boundary-layer before the interaction region. The separation shock affects the upstream flow at the point of influence U and the wall pressure rises effectively across the separation shock at primary separation point S1. It remains constant in the separated vortex flow and rises to peak values at primary reattachment R1. The wall pressure then decreases away from the reattachment region and rises near the fin-plate junction. The skin friction does not vary significantly in the unperturbed boundary-layer before the region of influence U. The boundary-layer is compressed across the separation shock wave, hence it increases the velocity gradient and thereby increases skin

friction. The skin friction reaches a peak value at the reattachment point R1 due to the high values of the velocity gradient, hence shear stress.

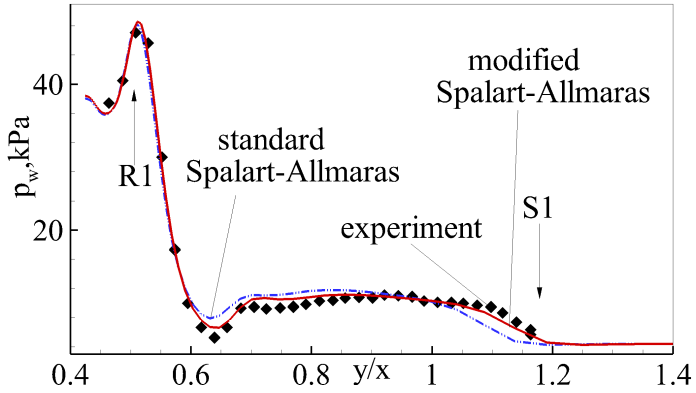

Figure 10. Comparison of computed wall pressure at x-section = 152 mm with experiments [19] using standard Spalart-Allmaras (SA) model [18] and modified Spalart-Allmaras model [16].

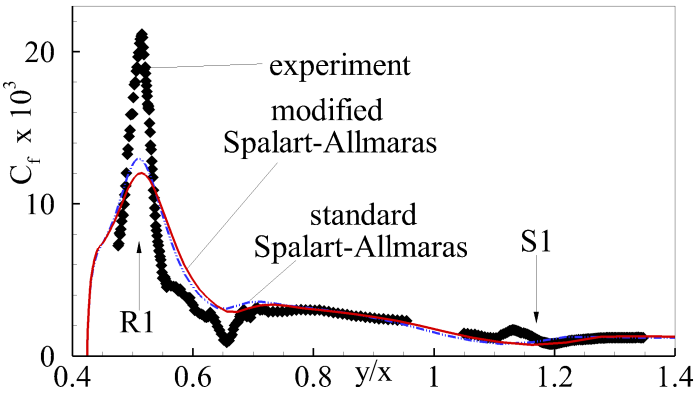

Figure 11. Comparison of computed skin friction at x-section = 122 mm with experiments [19] using standard Spalart-Allmaras (SA) model [18] and modified Spalart-Allmaras model [16].

Figure 10 indicates that at x-section = 152 mm, experiments give an initial pressure rise location at y/x = 1.22, where as the standard Spalart-Allmaras model predicts a delayed separation at y/x = 1.14. A similar trend is observed by the standard model at all other x-sections as shown in Table 1. A vortex region is calculated based on the distance between S1 and R1. The standard Spalart-Allmaras model predicts a small vortex region of 74 mm as compared to the experimental value of 82 mm. The skin friction coefficient predicted by the standard model in Figure 11 matches close to the experiments, except in the secondary flow separation region. The model also under-predicts the peak values in the reattachment region.

The shock-unsteadiness correction of [16] is applied to the complex region of three-dimensional shock/boundary-layer interaction by evaluating the shock-unsteadiness parameter c'_{b_1} in Eq. 1. It is a function of the upstream normal Mach number M_{1n} and needs to be evaluated at each shock wave so as to implement the shock-unsteadiness correction. The three-dimensional shock structure in the single fin configuration is quite complex. It is not easy to find the orientation of the different shock waves and the inclination of the upstream flow at each shock. Therefore, it is a difficult task to calculate the mean value of M_{1n}. An alternate approach is to use different values of c'_{b_1} in the current single fin case to improve the flow predictions. A similar approach by Gaitonde et al. [27] was used for simulating three-dimensional double-fin shock/boundary-layer interaction. The turbulence model constants were varied by limiting the value of production term in standard k-ϵ turbulence

Preprints (www.preprints.org) | NOT PEER-REVIEWED | Posted: 26 July 2017 doi:10.20944/preprints201707.0072.v1

Peer-reviewed version available at Arabian Journal for Science and Engineering 2018; doi:10.1007/s13369-018-3210-6

model. A smaller value of model constant resulted in lower turbulent kinetic energy. Hence, the computed solution resulted in a larger separated region and matched well with the experimental flowfield and wall pressure.

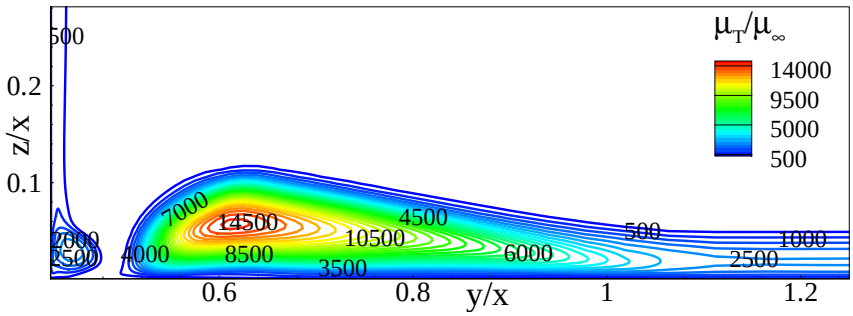

Figure 12. Computed normalized eddy-viscosity contours at x-section = 122 mm using standard Spalart-Allmaras model [18].

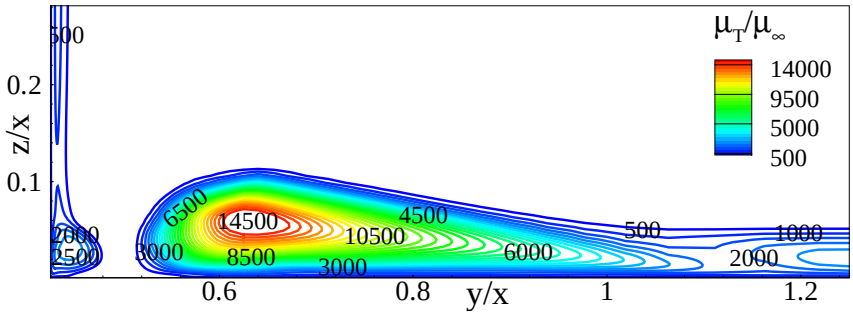

Figure 13. Computed normalized eddy-viscosity contours at x-section = 122 mm using shock-unsteadiness modified Spalart-Allmaras model [16].

Table 1. Comparision of primary separation point S1 and reattachment point R1 using standard Spalart-Allmaras (SA) and shock-unsteadiness modified SA model with the experiments [19] at different x-sections on the flat plate.

	S1			R1		
x-section, mm	**experiment**	**SA**	**modified SA**	**experiment**	**SA**	**modified SA**
82	1.3	1.24	1.3	-	0.5	0.5
92	1.27	1.22	1.27	-	0.51	0.51
122	1.23	1.16	1.21	-	0.51	0.51
152	1.22	1.14	1.2	0.52	0.52	0.52
162	-	1.13	1.18	-	0.51	0.51
182	-	1.12	1.15	0.52	0.52	0.52

In the present case, a shock-unsteadiness parameter of c'_{b_1} = -0.2 is chosen to yield a larger separation and is found to match the experimental initial pressure rise location closely as indicated in Figure 10. The shock-unsteadiness correction reduces the turbulent eddy viscosity in the region of the separation shock. This causes an increase in the length of the separation shock and hence brings the separation point predictions close to the experiments. The same trend is observed in the axisymmetric flows over cone-flare cases at hypersonic Mach numbers in Ref. [17].

Figures 12 and 13 indicate that the modification predicts lower values of μ_T/μ_∞ in the region of $y/x \simeq 1.2$, as compared to the standard Spalart-Allmaras model. Hence, the modified model improves the initial pressure rise location S1 (see Figure 10). Also, the pressure distribution is well predicted in the reattachment region and the corner region of the plate fin junction by the modified model as compared to the standard model.

Figure 11 depicts that the modified model over predicts the skin friction between $y/x = 0.65$ and 0.72. Whereas, it under predicts the skin friction by 42% at the reattachment region R1. Panaras [15] attributed this under prediction of skin friction due to the poor performance of turbulence models. The models indicated lower values of turbulence inside the separation vortices, making the flow almost laminar in this region. More advanced two-equation turbulence models [16**? ?**] can be applied to capture the velocity gradients, hence predict the peak skin friction at the reattachment region accurately. Currently, this is beyond the scope of work. The modified Spalart-Allmaras model predicts vortex region length between S1 and R1 to be 79 mm which is close to the experiment. The computed locations of primary separation point S1 and reattachment point R1 are compared with the experimental data at different x-sections in Table 1. Overall, the modified Spalart-Allmaras model matches to the experimental data at all locations.

6. Conclusion

Reynolds-averaged Navier-Stokes based computations were carried out to investigate the three-dimensional shock/boundary-layer interaction in a single fin configuration at Mach 5 with a large deflection angle of 23°. The shock-unsteadiness modified Spalart-Allmaras model and its standard version are used in the computations. The inviscid shock generated by the fin interacts with the boundary layer on the adjacent flat plate and results in a formation of a complex region. The viscous effects cause the bifurcation of inviscid shock and result in the formation of a lambda shock structure, one edge being the separation shock and the other being the rear shock. Type-IV shock-shock interaction results from the interaction of these shock waves. The lambda shock encloses a cross flow conical vortex. A shear-layer emanates from the separation point and interacts with the rear shock-wave and then rolls up and turns back to form a tongue. An entropy layer is generated at the triple point and a set of compression and expansion waves are embedded in it and the shear layer. These flow features influence the wall pressure and skin friction and a correlation between them is explained. The standard Spalart-Allmaras model predicts initial pressure location downstream of experiments. The shock-unsteadiness correction leads to an improvement in prediction of the initial pressure rise location. This leads to an accurate prediction of vortex size, hence the shock structure. The skin friction is under predicted at reattachment region in comparison to experiments by both the modified model and its standard version. This behavior is attributed to the poor performance of these models due to the prediction of laminar flow in this region. Further improvements to the present computations are envisaged by simulating the more advanced two-equation turbulence models.

7. Acknowledgment

The author would like to thank Prof. Krishnendu Sinha from Department of Aerospace Engineering, Indian Institute of Technology Bombay, for his valuable guidance, help and selflessness time investment to accomplish this work.

References

1. Bose, D., Brown, J. L., Prabhu, D. K., Gnoffo, P., Johnston, C. O., and Hollis, B. Uncertainty assessment of hypersonic aerothermodynamics prediction capability. *Journal of Spacecraft and Rockets* **2003** *50*(1) 12-18, DOI.
2. Marvin, J. G., Brown, J. L., and Gnoffo, P. A. Experimental database with baseline CFD solutions: 2-d and axisymmetric hypersonic shock-wave/turbulent boundary-layer interactions. NASA TM2013216604, 2013.

3. Yang Z. Large-Eddy simulation: past, present and the future. *Chinese Journal of Aeronautics* **2015** *28*(1) 11-24, DOI.
4. Kubota, H. and Stollery, J. An experimental study of the interaction between a glancing shock wave and a turbulent boundary layer. *Journal of Fluid Mechanics* **1982** *116* 431-58, DOI.
5. Alvi, F. S. and Settles, G. Physical model of the swept shock wave/boundary layer interaction flowfield. *AIAA Journal* **1992** *30*(9) 2252-2258, DOI.
6. Edwards, J. R. and Chandra, S. Comparison of eddy viscosity-transport turbulence models for three-dimensional shock-separated flowfields. *AIAA Journal* **1996** *34*(4) 756-763, DOI.
7. Panaras, A. G. The effect of the structure of swept-shock-wave/turbulent boundary-layer interactions on turbulence modeling. *Journal of Fluid Mechanics* **1997** *338* 203-230, DOI.
8. Thivet, F. Lessons learned from RANS simulations of shock wave/boundary layer interactions. AIAA Paper 2002-0583, Jan. 2002.
9. Panaras, A. G. Calculation of flows characterized by extensive crossflow separation. *AIAA Journal* **2004** *42*(12) 2474-2475, DOI.
10. Delery, J., Marvin, J. G. and Reshotko, E. Shock-wave boundary layer interactions. AGARDograph No. 280, ISBN 92-835-159-6, 1996.
11. Panaras, A. G. Review of the physics of swept-shock/boundary layer interactions. *Progress in Aerospace Sciences* **1996** *32* 173-244, DOI.
12. Knight, D. D., and Degrez, G. Shock wave turbulent boundary layer interactions in high mach number flows–a critical survey of current numerical prediction capabilities. AGARD Advisory Report **1998** *319*(2) pp. 1.1-1.35.
13. Knight, D., Yan, H., Panaras, A. G., and Zheltovodov, A. Advances in CFD prediction of shock wave turbulent boundary layer interactions. *Progress in Aerospace Sciences* **2003** *39*(2-3) 121-184, DOI.
14. Babinsky, H. and Harvey, J. K. In *Shock wave-boundary-layer interactions*; Cambridge University Press, 2011.
15. Panaras, A. G. Turbulence modeling of flows with extensive crossflow separation. *Aerospace* **2015** *2*(3) 461-481, DOI.
16. Sinha, K., Mahesh, K., and Candler, G. V. Modeling the effect of shock-unsteadiness in shock/turbulent boundary-layer interactions. *AIAA Journal* **2005** *43*(3) 586-594, DOI.
17. Pasha, A. A., and Sinha, K. Shock-unsteadiness model applied to hypersonic shock wave/turbulent boundary-layer interactions. *Journal of Propulsion and Power* **2012** *28*(1) 46-60, DOI.
18. Spalart, P. R., and Allmaras, S. R. A one-equation turbulence model for aerodynamic flows. AIAA Paper 1992-0439, 1992.
19. Schulein, E. Optical skin friction measurements in short-duration facilities. *AIAA Journal* **2006** *44*(8) 1732-1742, DOI.
20. Wilcox, D. C. In *Turbulence modeling for CFD*; La Canada, CA: DCW Industries, 2nd ed., 2000, pp. 491-492.
21. Sinha. K., Candler G.V., Convergence improvement of two-equation turbulence model calculations. AIAA Paper,AIAA-98-2649, 1998.
22. Pasha, A. A. and Sinha, K. Shock-Unsteadiness model applied to oblique shock-wave/turbulent boundary-layer interaction. *International Journal of Computational Fluid Dynamics* **2008** *22*(8) 569-582, DOI.
23. siva:2009 Reddy, D. S. K. and Sinha, K. Hypersonic turbulent flow simulation of fire II re-entry vehicle afterbody. *Journal of Spacecraft and Rockets* **2009** *46*(4) 745-757, DOI.
24. Edney, B. E. Anomalous heat transfer and pressure distributions on blunt bodies at hypersonic speeds in the presence of an impinging shock. The Aeronautical Research Institute of Sweden, Stockholm, FFA Rept. 115, Feb. 1968.
25. Catris, S. and Aupoix, B. Density corrections for turbulence models. *Aerospace Science and Technology* **2000** *4*(1) 1-11, DOI.
26. Deck, S., Duveau, P., d'Espiney, P., and Guillen, P. Development and application of SpalartAllmaras one-equation turbulence model to three-dimensional supersonic complex configurations. *Aerospace Science and Technology* **2002** *6*(3) 171-183, DOI.
27. Gaitonde, D. V. Progress in shock-wave/boundary-layer interactions. *Progress in Aerospace Sciences* **2015** *721* 80-99, DOI.
28. Quadros, R., Sinha, K., and Larsson, J. Turbulent energy flux generated by shock/homogeneous turbulence interaction. *Journal of Fluid Mechanics* **2016** *976* 113-157, DOI.

303 29. Quadros, R., and Sinha, K. Modelling of turbulent energy flux in canonical shock-*International Journal of*
304 *Heat and Fluid Flow* **2016** *61* 626-635, DOI.